

# Barchan dune asymmetry: Numerical investigation

Eric J. R. Parteli<sup>a</sup>, Orencio Durán<sup>b</sup>, Mary C. Bourke<sup>c,d</sup>, Haim Tsoar<sup>e</sup>, Thorsten Pöschel<sup>a</sup>, Hans J. Herrmann<sup>f,g</sup>

<sup>a</sup>*Institut für Multiscale Simulation, Universität Erlangen-Nürnberg, Nögelsbachstr. 49b, 91052, Erlangen, Germany*

<sup>b</sup>*Department of Geological Sciences, University of North Carolina-Chapel Hill, Chapel Hill, NC, USA*

<sup>c</sup>*Planetary Science Institute, 1700 E Ft Lowell, #106, Tucson AZ, USA*

<sup>d</sup>*Department of Geography, Trinity College Dublin, Ireland*

<sup>e</sup>*Dep. Geogr. Environ. Development, Ben-Gurion Univ. Negev, Beer Sheva 84105, Israel*

<sup>f</sup>*Institut für Baustoffe IfB, ETH Hönggerberg, HIF E 12, CH-8093, Zürich, Switzerland.*

<sup>g</sup>*Departamento de Física, Universidade Federal do Ceará - 60455-760, Fortaleza, Ceará, Brazil*

---

## Abstract

Barchan dunes — crescent-shaped dunes that form in areas of unidirectional winds and low sand availability — commonly display an asymmetric shape, with one limb extended downwind. Several factors have been identified as potential causes for barchan dune asymmetry on Earth and Mars: asymmetric bimodal wind regime, topography, influx asymmetry and dune collision. However, the dynamics and potential range of barchan morphologies emerging under each specific scenario that leads to dune asymmetry are far from being understood. In the present work, we use dune modeling in order to investigate the formation and evolution of asymmetric barchans. We find that a bimodal wind regime causes limb extension when the divergence angle between primary and secondary winds is larger than  $90^\circ$ , whereas the extended limb evolves into a seif dune if the ratio between secondary and primary transport rates is larger than 25%. Calculations of dune formation on an inclined surface under constant wind direction also lead to barchan asymmetry, however no seif dune is obtained from surface tilting alone. Asymmetric barchans migrating along a tilted surface move laterally, with transverse migration velocity proportional to the slope of the terrain. Limb elongation induced by topography can occur when a barchan crosses a topographic rise. Furthermore, transient asymmetric barchan shapes with extended limb also emerge during collisions between dunes or due to an asymmetric influx. Our findings can be useful for making quantitative inference on local wind regimes or spatial heterogeneities in transport conditions of planetary dune fields hosting asymmetric barchans.

**Keywords:** Barchan dunes, Dune asymmetry, Wind erosion, Sand transport, Dune model

---

## 1. Introduction

The classical symmetric shape of barchan dunes is far from being prevalent in nature. A wide variety of barchan morphologies on Earth and Mars are asymmetric, with one limb extended downwind (Tsoar, 1984; Bourke, 2010). Since the pioneering works by Bagnold (1941), various conceptual models have been proposed in order to explain the existing asymmetric dune morphologies. Dune asymmetry has been most predominantly attributed to asymmetric bimodal winds, topography, dune collisions or asymmetric sand influx. Indeed, understanding dune asymmetry constitutes an important issue in planetary science, as asymmetric dunes could potentially serve as a proxy for local wind regimes or variations in sand supply or topography. However, the significance of the different causes of barchan asymmetry is still poorly understood, whereas the potential range of dune morphologies resulting in each case remains unknown. Although some insights into the

dynamics of asymmetric dunes could be gained from field monitoring within a time span of a few years (Bourke, 2010), assessment of dune shape evolution is a difficult task owing to the long timescales involved in dune processes. Moreover, diverse asymmetric dune morphologies (Bourke et al., 2004; Bourke and Goudie, 2009) might be the outcome of different factors in concurrent action, which poses a further challenge in the investigation of the developmental stages of asymmetric dunes through field observations.

Numerical modeling — which has become indispensable in the investigation of aeolian and dune processes on Earth and other planetary bodies (Bourke et al., 2010; Kok et al., 2012) — could provide a helpful tool in the study of barchan dune asymmetry. In order to shed light on the factors competing for the appearance of various asymmetric dune shapes, a minimal model that accounts for a mathematical description of the wind over dunes, as well as for the equations for grain transport and landscape evolution is required. Such a model has been developed in the course of the last decade (Sauermaun et al., 2001; Kroy et al., 2002; Durán and Herrmann, 2006a;

---

*Email address:* Eric.Parteli@cbi.uni-erlangen.de (Eric J. R. Parteli)

Durán et al., 2010). This model combines an analytical model for the average turbulent flow over the sand landscape with a continuum model for sand transport. The model has proven to reproduce the shape of different types of dunes with good quantitative agreement with measurements (Sauermann et al., 2003; Durán and Herrmann, 2006a,b; Parteli and Herrmann, 2007). The model has been further extended in order to model longitudinal seif dunes and diverse unusual Martian dune forms under bimodal wind regimes (Parteli et al., 2009).

In the present work, we use the dune model to investigate the role of different asymmetry causes for the diversity of asymmetric barchan shapes reported previously from observations of dune fields on Earth and Mars (Bourke, 2010). We calculate the evolution of a symmetric barchan dune under the separate action of the potential causes for dune asymmetry.

This paper is organized as follows. In Section 2 the dune model is described. In Sections 3-6 we present and discuss the results obtained from calculations of barchan dune asymmetry due to bimodal wind regimes, topography, asymmetric sand supply and dune collision, respectively. Conclusions are presented in Section 7.

## 2. Model description

The model used in the calculations of the present work consists of a set of mathematical equations that compute: the average turbulent wind field (the surface shear stress ( $\boldsymbol{\tau}$ ) over the topography; the mass flux ( $\mathbf{q}$ ) of saltating particles due to the shear stress, and the time evolution of the surface resulting from particle transport (Sauermann et al., 2001; Kroy et al., 2002; Durán and Herrmann, 2006a). In this Section, we present a brief description of the model equations and of the calculation procedure.

### 2.1. Wind field

The first step consists of describing quantitatively the average three-dimensional turbulent wind field over the dune. The average shear stress field ( $\boldsymbol{\tau}$ ) is calculated through solving a set of analytical equations developed by Weng et al. (1991).

In the absence of dunes, the wind velocity  $\mathbf{v}(z)$  within the atmospheric boundary layer increases logarithmically with the height ( $z$ ) above the flat ground, i.e.  $\mathbf{v}(z) = 2.5 \mathbf{u}_{*0} \ln(z/z_0)$ , where the wind shear velocity  $\mathbf{u}_{*0}$  is used to define the (undisturbed) shear stress  $\boldsymbol{\tau}_0 = \rho_{\text{fluid}} |\mathbf{u}_{*0}| \mathbf{u}_{*0}$ , and  $\rho_{\text{fluid}}$  is the air density. A smooth hill or dune introduces a perturbation in the wind field. The Fourier-transformed longitudinal and transverse components of the shear stress perturbation ( $\hat{\boldsymbol{\tau}}$ ) due to the local topography are computed using following equations,

$$\hat{\tau}_x = \frac{\tilde{h}_s k_x^2}{|\vec{k}|} \frac{2}{U^2(l)} \left\{ -1 + \left( 2 \ln \frac{l}{z'_0} + \frac{|\vec{k}|^2}{k_x^2} \right) \sigma \frac{K_1(2\sigma)}{K_0(2\sigma)} \right\}, \quad (1)$$

$$\hat{\tau}_y = \frac{\tilde{h}_s k_x k_y}{|\vec{k}|} \frac{2}{U^2(l)} 2\sqrt{2}\sigma K_1(2\sqrt{2}\sigma), \quad (2)$$

where  $x$  and  $y$  are parallel, respectively, perpendicular to the wind direction,  $\sigma = \sqrt{i L k_x z_0 / l}$ ,  $k_x$  and  $k_y$  are the components of the wave vector  $\vec{k}$ , i.e. the coordinates in Fourier space,  $K_0$  and  $K_1$  are modified Bessel functions and  $\tilde{h}_s$  is the Fourier transform of the height profile;  $U$  is the vertical velocity profile which is suitably non-dimensionalized,  $l$  is the depth of the inner layer of the flow and  $L$  is a typical length scale of the hill or dune and is given by  $1/4$  the mean wavelength of the Fourier representation of the height profile. In the presence of the saltating grains, the roughness of the dune's surface increases to an apparent value  $z'_0$ , the aerodynamic roughness (Bagnold, 1941). The wind velocity over the dune is calculated using  $z'_0 = 1$  mm, a value based on experimental observations (Bagnold, 1941; Andreotti, 2004). The surface shear stress field is obtained, then, with the equation,

$$\boldsymbol{\tau} = |\boldsymbol{\tau}_0| (\boldsymbol{\tau}_0 / |\boldsymbol{\tau}_0| + \hat{\boldsymbol{\tau}}), \quad (3)$$

where  $\boldsymbol{\tau}_0$  is the undisturbed shear stress over the flat ground.

Flow separation at the dune brink due to the strong local curvature of the surface gives rise to a zone of recirculating flow (Walker and Nickling, 2002; Herrmann et al., 2005), which cannot be described by the analytical model (Weng et al., 1991). This problem is overcome introducing the so-called “separation bubble”: for each longitudinal slice of the dune, a separation streamline connecting the brink to the reattachment point is introduced at the lee. Each separation streamline is fitted to a third-order polynomial, the parameters of which are determined as described in detail by Kroy et al. (2002). The wind model (Weng et al., 1991) is then solved for the smooth “envelope” that comprises the separation bubble and the dune surface (Kroy et al., 2002). Thereafter, the shear stress in the recirculating zone within the separation bubble is set as zero, since the net transport within the bubble essentially vanishes.

### 2.2. Sand flux

Next, the mass flux of particles in saltation — which is the dominant transport mode and consists of grains hopping in ballistic trajectories and ejecting new particles upon collision with the ground — is computed. The saltation cloud is regarded as a thin, fluid-like layer that can exchange sand with the immobile sand bed (Sauermann et al., 2001).

When the wind shear stress exceeds a minimal threshold and saltation begins, the sand flux first grows exponentially due to the multiplicative process inherent to the saltation process. However, since saltating grains accelerate at cost of aeolian momentum, the flux cannot increase beyond a maximal value, the so-called saturated sand flux (Bagnold, 1941; Sauermann et al., 2001; Almeida et al.,

2008; Durán et al., 2011; Pähtz et al., 2012) which is reached after a saturation transient where the air shear stress within the saltation cloud equals the minimal value for sustained saltation, i.e. the impact threshold,  $\tau_t = \rho_{\text{fluid}} u_{*t}^2$  (Bagnold, 1941), defined in terms of the impact threshold shear velocity  $u_{*t}$ . In the continuum model, the derivation of the three-dimensional equations for the sand flux is performed by explicitly accounting for the decrease in aeolian shear stress due to the growth of the number of particles in saltation (the “feedback effect” (Owen, 1964)), which leads to the saturation transient of the flux as described above. The following equation is obtained for the sand flux ( $\mathbf{q}$ ) over the terrain,

$$\nabla \cdot \mathbf{q} = (1 - |\mathbf{q}|/q_s)|\mathbf{q}|/\ell_s, \quad (4)$$

where  $q_s = [2\alpha|\mathbf{v}_s|/g](\tau - \tau_t)$  is the saturated flux;  $\ell_s = [2\alpha|\mathbf{v}_s|^2/g\gamma]\tau_t(\tau - \tau_t)^{-1}$  is the characteristic length of flux saturation;  $g$  is gravity;  $\alpha \approx 0.4$  and  $\gamma \approx 0.2$  are empirically determined model parameters (Sauermann et al., 2001; Durán and Herrmann, 2006a), and the steady-state velocity of the particles in saltation ( $\mathbf{v}_s$ ) is calculated numerically from the balance between aeolian drag, gravitational and bed friction forces on the particles (Durán et al., 2010). The outcome of the calculation is a two-dimensional field ( $\mathbf{q}(x, y)$ ) that gives the height-integrated, average mass flux of saltating particles over the terrain.

### 2.3. Surface evolution

Finally, mass conservation is used in order to compute the evolution of the local height ( $h(x, y)$ ) through the equation,

$$\rho_{\text{sand}} \partial h / \partial t = -\nabla \cdot \mathbf{q}, \quad (5)$$

where  $\rho_{\text{sand}}$  is the bulk sand density. Eq. (5) implies that the deposition (erosion) occurs at those places where the flux locally decreases (increases) downwind.

*Avalanches* — wherever the local slope exceeds the angle of repose of the sand ( $\theta_c \approx 34^\circ$ ), the surface is relaxed through avalanches in the direction of the steepest descent. Avalanches are considered to be instantaneous as their time-scale can be regarded as negligible compared to the time-scale of the surface evolution due to aeolian transport. The flux of avalanches along the slip-face is given by,

$$\mathbf{q}_{\text{aval}} = k[\tanh(\nabla h) - \tanh(\theta_{\text{dyn}})] \frac{\nabla h}{|\nabla h|}, \quad (6)$$

where  $k = 0.9$  is a parameter and  $\theta_{\text{dyn}} = 33^\circ$  is the so-called “dynamic” angle of repose, which characterizes the surface after relaxation (Durán et al., 2010). The update in the local height is obtained by solving Eq. (5) using the flux due to avalanches given by Eq. (6). The calculation is repeated until the local slope is below  $\theta_{\text{dyn}}$ .

### 2.4. Description of the calculation procedure

Summarizing, the model consists of iteratively performing the following calculations:

1. the average shear stress ( $\tau$ ) over the surface is computed using Eqs. (1), (2) and (3);
2. next, the height-integrated average mass flux  $\mathbf{q}$  over the terrain is calculated by solving Eq. (4);
3. the change in the local surface is computed with Eq. (5); wherever the local inclination is larger than  $34^\circ$ , the flux due to avalanches is calculated using Eq. (6) and the topography updated again using Eq. (5).

The initial surface is a smooth hill of Gaussian shape, which is subjected to a constant upwind shear stress of value  $\tau_0$  — in the following, we call the upwind shear stress simply  $\tau$ . Calculations are performed with open boundaries and an influx  $q_{\text{in}}$  at the inlet, which is typically 20% of the saturated flux,  $q_s$  (Fryberger et al., 1984).

## 3. Bimodal wind regimes

Most attempts to model barchan asymmetry have concentrated on the role of asymmetric bimodal wind regimes for the elongation of one barchan limb. The bimodal wind is said to be asymmetric when the transport rates of both wind components are not equal.

The first conceptual model was by Bagnold (1941). According to this model, a symmetric barchan, originally formed by a gentle wind, becomes asymmetric if a storm wind blows from a secondary direction, making an acute divergence angle with the primary one. The limb exposed to the storm wind elongates as it enters the sand stream of the limb at the opposite side, thus evolving into a longitudinal seif dune (McKee and Tibbitts, 1964; Tsoar, 1982, 1983; Bristow et al., 2000; Rubin et al., 2008; Tokano, 2010). According to Bagnold’s model, the seif dune formed in this manner aligns approximately parallel to the direction of the storm (Bagnold, 1941). This conceptual model was referred to by many authors in the past (Verstappen, 1968; Ruhe, 1975; Goudie and Wilkinson, 1977; Mabbutt, 1977; Lancaster, 1980), though reports on supporting field examples were scarce (Lancaster, 1980). A different model was proposed later by Tsoar (1984): a gentle wind (not a storm wind) blows from the secondary direction, and the limb that elongates is the one opposite to the secondary gentle wind (Tsoar, 1984). Some field observations exist that support this model (Bourke, 2010).

In our calculations, we simulate a bimodal wind by periodically alternating the orientation of the field between two directions forming a divergence angle,  $\theta_w$  (Parteli et al., 2009) — such as in the turntable experiments of ripples and subaqueous dune formation on a sediment bed under bimodal flow regimes (Rubin and Hunter, 1987; Rubin and Ikeda, 1990). The wind model is solved considering a constant wind blowing over the rotated landscape, while the separation bubble adapts to the wind direction following the rotation of the field (Parteli et al.,

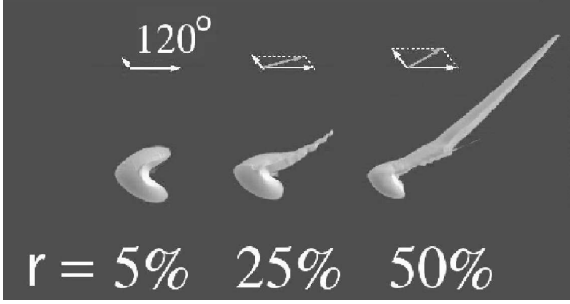


Figure 1: Elongation of one barchan limb due to a bimodal wind regime with obtuse divergence angle. Wind directions are indicated by the arrows (the primary wind, which has duration  $T_{w1}$ , blows from the left). The barchan shape depends on  $r = T_{w2}/T_{w1}$ , i.e. the duration  $T_{w2}$  of the secondary wind relative to  $T_{w1}$ . In these simulations,  $T_{w1}$  is about 3% of the migration time of the barchan dune,  $T_m$ . The shapes shown for  $r \leq 25\%$  are *stationary* shapes, whereas for  $r > 25\%$ , the elongated dune horn increases with time. Simulation snapshots correspond to time  $t$  of the order of  $5T_m$ . The barchan obtained in the simulation with  $r = 5\%$  has length and width of approximately 120 m.

2009). The *primary* wind direction, i.e. the one that forms the barchan, has duration  $T_{w1}$  and upwind shear stress  $\tau_1$ . The *secondary* wind direction makes an angle  $\theta_w$  with the primary wind, and lasts for a time  $T_{w2}$  with upwind shear stress  $\tau_2$ .

We begin our study with an obtuse divergence angle ( $\theta_w = 120^\circ$ ), and consider two models:

*Model #1:* both wind directions have the same upwind shear stress ( $\tau_1 = \tau_2$ ), however the primary wind has a longer duration ( $T_{w1} > T_{w2}$ ) — a scenario reminiscent of the experiments by Rubin and Hunter (1987) with the difference, however, that in the simulations the ground is not covered with sand. Figure 1 shows snapshots of the dune evolution obtained from the calculations. As can be seen from Fig. 1, the barchan develops an asymmetric shape, which depends on the ratio  $r \equiv T_{w2}/T_{w1}$ . If  $r > 25\%$ , then the limb at the side opposite to the secondary wind elongates into the *resultant* wind direction (Fig. 1) to form a longitudinal dune. It is interesting that the longitudinal alignment also appears to be lost in turntable experiments of ripples on a sand bed when the transport rates differ by a factor larger than 4 (Rubin and Hunter, 1987). When  $r = 1.0$ , the barchan dune gives place to a symmetric longitudinal dune (Parteli et al., 2009).

*Model #2:* the primary wind has a larger shear stress ( $\tau_1 > \tau_2$ ) — as in the conceptual model by Tsoar (1984) — while  $T_{w1} = T_{w2}$ . In this case, the dune shapes do not differ much from the ones in Fig. 1. The limb opposite to the secondary wind elongates when the relative values of bulk sand flux in the secondary and primary wind directions,

respectively  $Q_2$  and  $Q_1$ , are such that  $r \equiv Q_2/Q_1 > 25\%$ . Indeed, we also considered the situation where the storm wind is the secondary one ( $Q_2 > Q_1$ ), such as in the model by Bagnold (1941). In this case, primary and secondary winds simply exchange their roles, whereas the same dune shapes such as in Fig. 1 are obtained. In summary, Bagnold’s hypothesis that the elongating limb is the one exposed to a secondary storm wind is not supported by the simulation results.

In a general manner, the condition for elongation of the asymmetric limb due to a bimodal wind of obtuse divergence angle, as found from our calculations, reads:

$$r \equiv [Q_2 \cdot T_{w2}]/[Q_1 \cdot T_{w1}] > 1/4, \quad (7)$$

where the indices 1 and 2 refer to the primary and to the secondary wind, respectively. Equation (7) allows us to estimate the onset for emergence of asymmetry in barchan dunes, where both the relative duration and shear stress values of the wind components are accounted for quantitatively.

Next, we extend the calculations to different values of the divergence angle  $\theta_w$ . In Fig. 2, the dune shape emerging from an asymmetric bimodal wind with  $r = 50\%$  is shown as a function of  $\theta_w$  and  $t_1 = T_{w1}/T_m$ , which is the duration of the primary wind,  $T_{w1}$ , rescaled by the migration or reconstitution time of the barchan,  $T_m \approx 0.02W^2/Q_1$  (Durán et al., 2010). The dune turnover time is roughly the time needed for the dune to cover a distance of its width ( $W$ ) (Allen, 1974; Lancaster, 1988; Rubin and Ikeda, 1990; Hersen et al., 2004).

As can be seen from Fig. 2, dunes orient transversely or longitudinally to the resultant transport trend, depending on whether  $\theta_w$  is acute or obtuse, respectively. Bimodal wind regimes with  $\theta_w < 90^\circ$  lead to rounded (or oblate) barchans, whereas larger values of  $\theta_w$  yield asymmetric dunes that elongate in the resultant transport direction (Parteli et al., 2009). However, the elongating limb is not stable if  $\theta_w$  is within the range  $90^\circ < \theta_w \lesssim 112^\circ$ . In this case, if the influx is sufficiently small, the extended limb separates from the barchan, giving rise to a “mixed state” (Rubin and Hunter, 1987; Rubin and Ikeda, 1990; Parteli et al., 2009), as depicted in Fig. 3a. In fact, mixed states analogous to the ones found for asymmetric barchans have been also found in turntable experiments of aeolian ripples and subaqueous bedforms on a sand bed for the same range of  $\theta_w$  (Rubin and Hunter, 1987; Rubin and Ikeda, 1990). At very large divergence angles, the resulting morphology resembles an asymmetric dune of “slim” shape (Long and Sharp, 1964; Bourke, 2010), as shown in the diagram of Fig. 2 and also illustrated with the calculation using  $\theta_w = 170^\circ$  in Fig. 3c. The dunes in Fig. 3c are “reversing” dunes, which are formed by winds coming from opposing directions. This dune form has been discussed by Tsoar (2001), who also gave examples of reversing dunes occurring in South Africa (Tsoar, 2001).

Asymmetric barchans such as the ones in Fig. 1 form when the relative duration of the primary wind ( $t_1 \equiv$

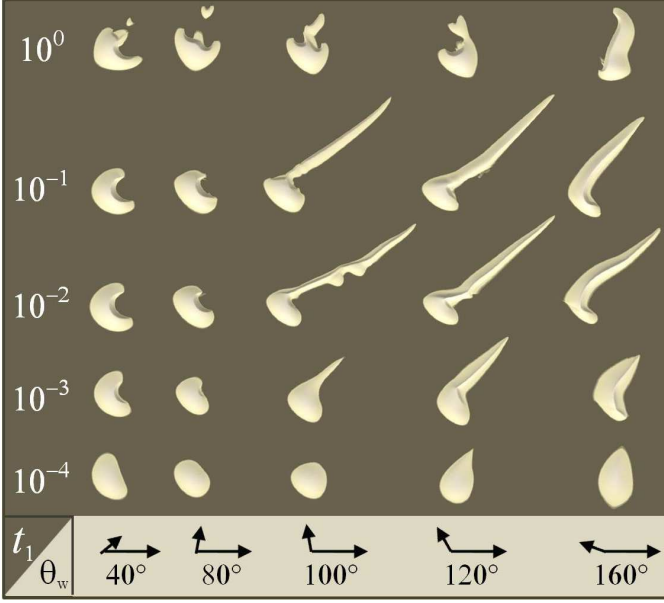


Figure 2: Dune shape as a function of the divergence angle ( $\theta_w$ ) of the bimodal wind, and of the rescaled duration of the primary wind ( $t_1 \equiv T_{w1}/T_m$ ), for  $r = 50\%$ . The directions of primary and secondary winds are indicated by the arrows (primary wind blows to the right). Simulation snapshots correspond to time  $t \approx 3T_m$ , except those obtained with  $t_1 = 10^{-4}$ , which correspond to time  $t \approx 0.2T_m$ .

$T_{w1}/T_m$ ) is within the range  $10^{-3} \lesssim t_1 \lesssim 10^{-1}$ . When  $t_1$  is smaller than about 0.1%, no limb elongation occurs; both limbs, as well as the slip face, disappear and a dome-like shape is obtained (c.f. Fig. 2). As  $t_1$  approaches unity, any change due to the secondary wind is fully compensated by the primary wind during every cycle of the bimodal wind regime — the resulting morphology is essentially a barchan that is periodically reformed by a unimodal wind of strength  $\tau_1$ , as can be seen from Fig. 2. The dune shapes shown in Fig. 2 for  $t_1 = 1.0$  are thus “transitional” shapes (de Hon, 2006). The oblique incidence of the secondary wind leads to destabilization of the dune surface and the emergence of smaller barchans, which detach from the larger dune and migrate on the bedrock thereby alternating between both directions of the bimodal wind. Figure 3b shows the calculation of a barchan under asymmetric bimodal wind regime with  $\theta_w = 120^\circ$  for  $t_1 = 1.0$  (top) and  $t_1 = 0.1$  (bottom). On the basis of Fig. 3b, it is possible to understand the coexistence of barchans and other complex bedforms shaped by multimodal wind regimes. If the dune is small enough, it has a small turnover time ( $\sim$  large  $t_1$ ) and can readapt to the prevailing transport trend notwithstanding the complexity of the wind system (Lancaster, 1988).

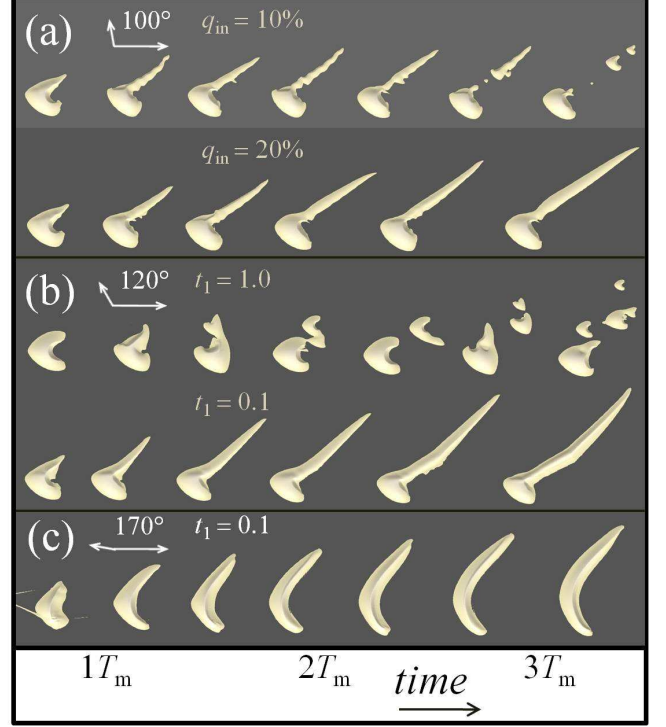


Figure 3: Time evolution of the barchan shape under bimodal wind regimes with obtuse divergence angle and  $r = 50\%$  (c.f. Fig. 2). Time is in units of the turnover time of the barchan ( $T_m$ ). (a) The divergence angle is  $\theta_w = 100^\circ$ , the duration of the primary wind (to the right) relative to  $T_m$  is  $t_1 = 0.1$ , and the influx ( $q_{in}$ ) is 10% (top) and 20% (bottom); (b)  $\theta_w = 120^\circ$ ,  $q_{in} = 20\%$ ,  $t_1 = 1.0$  (top) and 0.1 (bottom); (c)  $\theta_w = 170^\circ$ ,  $q_{in} = 20\%$ ,  $t_1 = 0.1$ .

#### 4. Topography

Field evidence of barchan limb elongation caused by topography are unclear (Finkel, 1959; Long and Sharp, 1964; Gay, 1999; Bourke, 2010). We investigate two cases where topography is observed to trigger dune asymmetry under both constant wind direction and sediment supply.

*Sloping terrain* — We consider a barchan dune migrating on a sloping terrain that makes an angle  $\varphi$  with the horizontal (Fig. 4a). The simulation starts with a symmetric barchan of height  $H$  and width  $W$ , which was shaped on a flat surface under constant upwind shear stress  $\tau$  and constant influx ( $q_{in}/q_s = 0.2$ ). Then, the barchan is let to evolve on the inclined surface. Due to gravity, sand transport on the tilted surface has now a component perpendicular to wind trend.

Figure 4b shows that the emerging barchan shape is asymmetric, yet none of its limbs elongate to form a longitudinal dune (Parteli et al., 2009; Reffet et al., 2010). The asymmetry arises from the combined effect of both downwind sand transport and gravity-driven mass flow in the direction orthogonal to the wind. Sand transport along the lower limb has a small net component downhill due

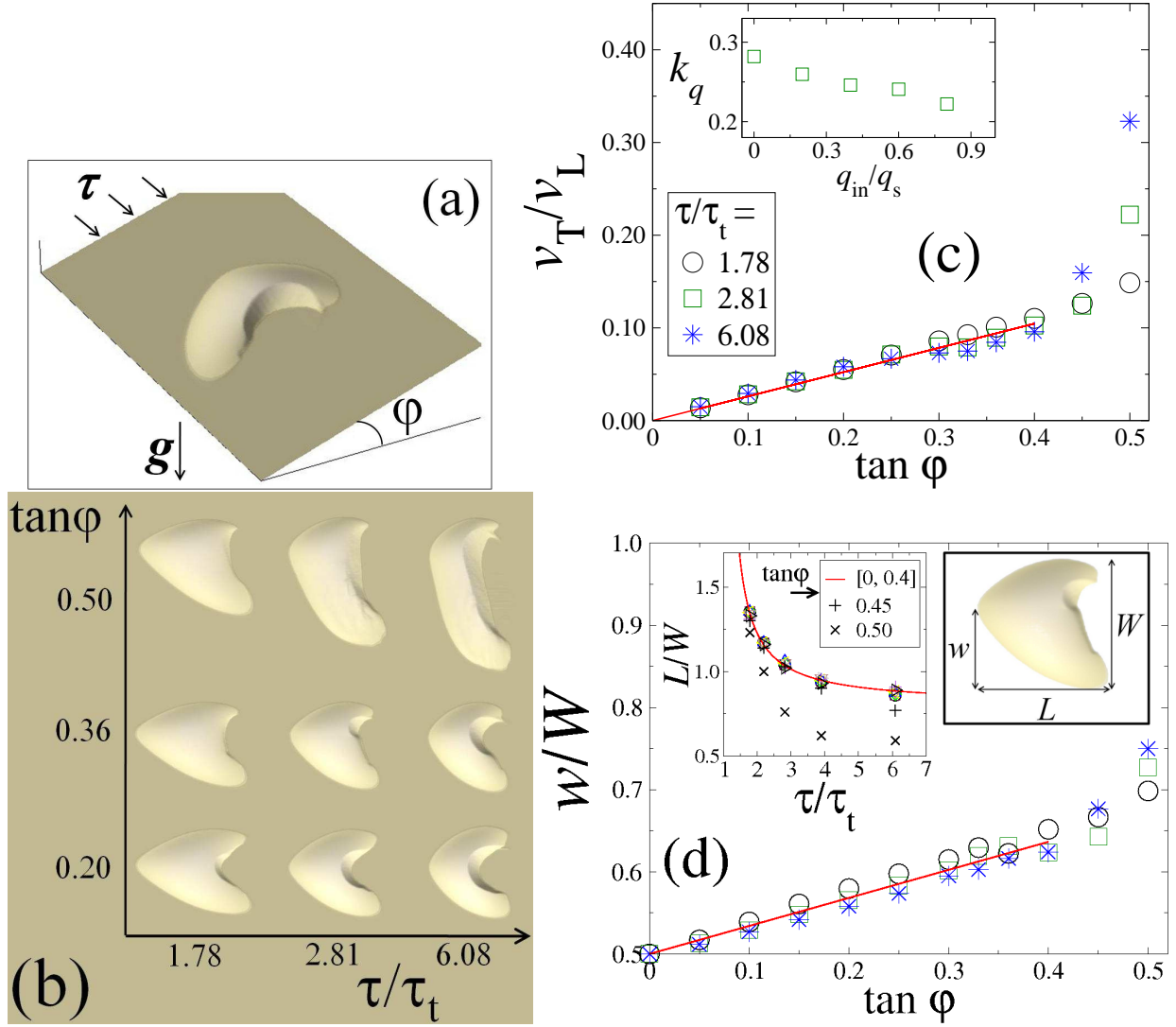


Figure 4: **(a)** Barchan dune of cross-wind width  $W \approx 90$  m migrating along a sloping terrain. The surface is tilted by an angle  $\varphi$ . Arrows indicate the wind direction ( $\tau$  is the upwind shear stress) and gravity ( $g$ ). **(b)** Dune shape as a function of  $\varphi$  and  $\tau/\tau_t$  (wind blows from left to right). Simulations were performed with  $q_{in}/q_s = 0.2$ . **(c)** Main plot: Ratio between transverse and longitudinal migration velocities, respectively  $v_T$  and  $v_L$ . The best fit to the data using the equation  $v_T/v_L = k_q \tan \varphi$  gives  $k_q \approx 0.26$  (continuous line). Inset:  $k_q$  as a function of  $q_{in}/q_s$ . **(d)** Main plot: The degree of asymmetry is quantified in terms of the ratio  $w/W$ , calculated as a function of the surface inclination ( $\varphi$ ) and for the same values of  $\tau/\tau_t$  shown in the main plot of (a). Inset: Length-to-width ratio ( $L/W$ ) as a function of  $\tau/\tau_t$  calculated for different values of  $\varphi$  within the range  $0 < \tan \varphi < 0.4$  and for two values of  $\varphi$  above this range ( $\varphi = 0.45$  and  $\varphi = 0.50$ ). The best fit to the data within the range  $0 < \tan \varphi < 0.4$  using the equation  $L/W \approx A[\tau/\tau_t - 1]^{-1} + B$  gives  $A \approx 0.42$  and  $B = 0.8$  (continuous line).

to the tilting, and so this limb stretches downhill. In contrast, the upper limb is not stretched because the sand transported laterally due to the tilting is trapped at the slip face.

A consequence of the surface inclination is the downhill extension of the barchan. The migration velocity of the barchan dune orthogonal to the wind trend increases with  $\varphi$ , as shown in the main plot of fig. 4c. For moderate

values of  $\varphi$  within the range  $0 \leq \tan \varphi \leq 0.4$ , the ratio between transverse and longitudinal migration velocities,  $v_T$  and  $v_L$ , respectively, can be described by the equation:

$$v_T/v_L = k_q \tan \varphi, \quad (8)$$

where the coefficient  $k_q \approx 0.26$  has a slight dependence on the upwind sand flux,  $q_{in}/q_s$  (c.f. inset of fig. 4c). The ratio  $v_T/v_L$  for barchans migrating on a sloping terrain is



thus a function of the slope  $\varphi$ , being independent of the wind velocity.

The topography-induced barchan asymmetry can be quantified in terms of the relative width  $w/W$ , where  $W$  is the total dune width, and the width  $w$  is the distance — measured in the direction orthogonal to wind trend — between the border of the dune at the lowest elevation and the dune’s windward foot (c.f. fig. 4d). If there is no surface tilting ( $\varphi = 0$ ), then  $w = 0.5$  since the dune is symmetric along its central axis. As  $\varphi$  increases within the range  $0 \leq \tan\varphi \leq 0.4$ ,  $w$  increases roughly linearly with  $\tan\varphi$ , as shown in fig. 4d. Within this moderate range of  $\varphi$ , the ratio  $w/W$  can be described by the equation,

$$w/W = k_w \tan\varphi, \quad (9)$$

where the value  $k_w \approx 0.33$  is obtained from the best fit to the simulation data (c.f. Fig. 4d). The aspect ratio of the dune ( $L/W$ ), which is a function of the relative shear stress ( $\tau/\tau_t$ ) (Kroy et al., 2002; Parteli et al., 2007), is essentially independent of  $\varphi$ . In other words,  $\tau/\tau_t$  and  $\varphi$  can be approximately estimated from  $L/W$  and  $w/W$  of the asymmetric barchan shape, respectively, provided other asymmetry causes (i.e. bimodal wind, dune collisions or influx asymmetry) are not relevant at the dune field considered.

*Topographic rise* — Asymmetric barchans occasionally occur approaching and crossing a topographic break in slope (Bourke, 2010). We investigate, using the dune model, the evolution of a barchan crossing a ridge that is placed obliquely to the direction of motion (Fig. 5). The dune is subjected to a unimodal wind regime and an influx that is 20% of the saturated flux. We consider that the longitudinal axis of the ridge forms a moderate angle with the direction orthogonal to the wind (about  $45^\circ$ ). The ridge has Gaussian cross section, width  $L_r$  and height  $H_r$ , while the barchan has a height  $H \approx 9$  m.

Indeed, the height-to-width ratio  $H_r/L_r$  (or aspect ratio) of the ridge cannot be too large, as the ridge would act as a barrier for sand transport. On the contrary, a ridge of too small aspect ratio has negligible effect on the dune shape. An asymmetric dune shape with limb elongation occurs when the aspect ratio of the ridge is about  $1/20$ . In Figs. 5b and 5c, the ridge has height  $H_r = 7$  m and width  $L_r \approx 150$  m. As the barchan approaches the ridge, deposition occurs at the lee of the ridge, on the side corresponding to the closest limb. This limb then elongates once it arrives at the lee of the obstacle. The taller the ridge, the more accentuated the extension. As the other limb approaches sufficiently close to the ridge, a similar process occurs and thus that limb also elongates.

The deposition at the ridge’s lee occurs due to a decrease in wind strength just downwind of the crest. When the sand released through the limbs crosses the ridge’s crest, it cannot escape the lee since the transport rate there is reduced. As the dune advances and more limb sand is deposited, the wind strength at the lee suffices to extend

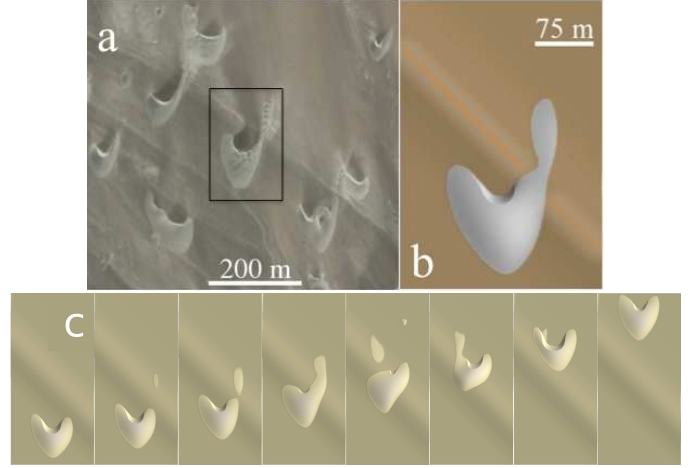


Figure 5: The potential influence of topography in the development of barchan asymmetry in Peru. (a) Barchan dunefield migrating across a landscape where resistant layers in underlying bedrock protrude as low ridges. Illumination is from the top and north is to the top of the image. The box indicates a barchan that extends its eastern limb across the topographic rise. Wind regime in the area is bimodal resulting in the extension of western limbs, except where influenced by topography. Images used with permission from Google Earth. (b) Asymmetric barchan dune of height  $\sim 9$  m produced with the model using a topographic rise of Gaussian cross section which has along-wind width 200 m and height 6 m. (c) Simulation snapshots of the evolution of the barchan dune. Time increases from left to right and wind blows from the bottom. The simulation was performed with  $\tau/\tau_t \approx 3.9$  and  $q_{in}/q_s = 0.2$ .

the limb, yet accumulation ensues. Future studies should focus on the asymmetric dune resulting from simulations using different angles between ridge orientation and wind direction, as well as different shapes of the ridge. Indeed, the results of our calculations should be valid for ridges which have a smooth cross section. If the ridge’s cross section has a sharp edge, then flow separation occurs and the flow is diverted parallel to the ridge along the lee side (Tsoar, 2001). Due to the assumption of our model that net flow ceases within the separation zone, the sand deposited at the lee of a ridge with sharp edge cannot be transported at all. Thus, three-dimensional flow patterns at the lee of dunes or obstacles should be accounted for in the modeling of dune asymmetry when the topographic rise has a sharp slope (Tsoar, 2001).

The asymmetric barchans of the field example in the image in Fig. 5a display superimposed substructures or “sand-wave instabilities” (Elbelrhiti et al., 2005) indicating the presence of a secondary wind direction. Certainly, the presence of oblique winds play an important role for the shape of the elongating limb and of the barchan. However, our calculations show that such secondary winds are not a necessary ingredient for limb elongation, i.e. the

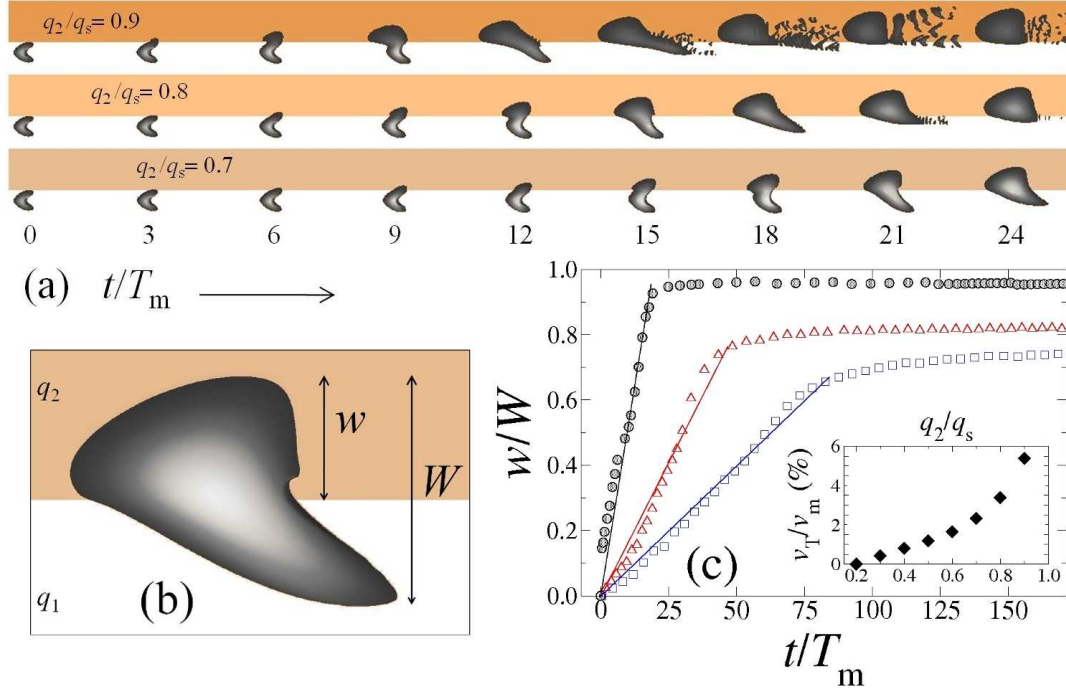


Figure 6: (a) Time evolution of a barchan of width 80 m subject to an asymmetric influx: The influx is  $q_1 = 20\%$  of  $q_s$  in the white areas, in the dark areas the influx is  $q_2$ , where  $q_2/q_s = 90\%$ ,  $80\%$  and  $70\%$ , respectively from top to bottom. The wind blows from the left with upwind shear stress  $\tau = 3.24\tau_t$ . Snapshots at time interval  $\Delta t = 3T_m$  where  $T_m$  is the turnover time of the barchan at  $t = 0$ . (b)  $w$  is the partial fraction of the barchan that is within the stream of larger influx ( $q_2 = 0.7$ ,  $t = 22T_m$ ), whereas  $W$  is the total width of the barchan. (c) Main plot:  $w/W$  as a function of time for  $q_2/q_s = 0.4$  (squares),  $0.6$  (triangles) and  $0.9$  (circles). The straight lines are the best fits to the simulation data using a linear relation  $w/W = kt/T_m$ , where  $k = v_T/v_m$  and  $v_T$  is the migration velocity in the direction orthogonal to wind. The inset shows that  $v_T$  is less than  $10\%$  of  $v_m$ .

asymmetric dune pattern in Fig. 5 can be explained only on the basis of a variation in wind strength induced by a topographic obstacle placed obliquely to the direction of motion. The asymmetric shape of dunes near a topographic rise can also be modified due to the presence of other dunes nearby, since different types of barchan asymmetry are generated by asymmetric influx or collisions between dunes, as will be discussed next.

## 5. Asymmetric sand supply

The role of asymmetric sediment supply for barchan asymmetry has remained uncertain in the few investigations undertaken (Rim, 1958; Lancaster, 1982; Bourke, 2010). It is admittedly a difficult task to conduct systematic field studies on the barchan shape as a function of the degree of spatial asymmetry in the upwind sediment budget. The sand flux onto the windward side of a barchan is largely dependent upon the spatial distribution of the upwind dunes or other sand sources, e.g. at a sand sea margin (Lancaster, 1982). Spatial inhomogeneities in the local physical properties of the interdune terrain may also play an important role for the incoming flux (Fryberger et al., 1984). Furthermore, the shape of a barchan migrating in

a field is inevitably affected by wind trend variations in time (Elbelrhiti et al., 2005), as well as by the interaction with neighbouring dunes through merging, breeding and lateral linking.

With the help of simulations, the barchan shape resulting from asymmetric upwind flux alone can be studied without regard to other physical factors. We consider a symmetric barchan initially migrating within an area where the influx  $q_1$  is approximately a constant fraction ( $\approx 20\%$ ) of the saturated flux ( $q_s$ ) — the value of  $q_1/q_s \approx 0.2$  is, in fact, within average values measured at interdune areas in typical barchan dune fields (Fryberger et al., 1984). The barchan has height  $H \approx 6.0$  m and width 80 m, and has been shaped by a constant shear stress  $\tau \approx 3.24\tau_t$ .

At  $t = 0$ , the upwind influx becomes asymmetric. The influx on the side of the barchan's left limb has a larger value,  $q_2 > q_1$  (dark areas in Fig. 6a). This model for asymmetric influx constitutes a simple model for a scenario typical for real dune fields, where in some areas the presence of a dome, a sand sheet or a larger dune migrating upwind may significantly increase the local interdune flux. Figure 6a shows different snapshots of the evolution of the barchan dune subject to the asymmetric influx. Because



more sand deposits in the areas of larger influx ( $q_2$ ), the dune adapts to the asymmetric influx by moving sideways towards the area where the influx is  $q_2$ . Different (transient) asymmetric dune shapes appear as the dune grows and moves sideways, as can be seen in Fig. 6a. The shorter limb is the one exposed to the larger influx value, because a large upwind flux prevents erosion at the windward foot and downwind motion of the dune. Thus, the barchan limb on the side of lower influx appears advanced in relation to its — “fat” (Long and Sharp, 1964; Parteli et al., 2007) — counterpart.

The fraction of the dune width ( $w/W$ , c.f. Fig. 6b) that is within the area of larger influx ( $q_2$ ) increases in time, as can be seen in Fig. 6c. The rate with which  $w/W$  grows in time is defined as the lateral migration velocity ( $v_T$ ) of the dune due to the asymmetric influx. Firstly,  $w/W$  increases roughly as a linear function of time which means that in this initial stage of lateral migration  $v_T$  is approximately constant for given values of  $q_1$  and  $q_2$  relative to  $q_s$ . The inset of Fig. 6c shows that  $v_T$  is indeed much smaller than the longitudinal migration velocity of the barchan ( $v_m$ ) even for large  $q_2/q_s$ . Indeed, the main plot of Fig. 6c suggests that, after a sufficiently long time,  $w/W$  asymptotically approaches a maximal value (and thus  $v_T \rightarrow 0$ ). Since the increase of  $w/W$  with time becomes extremely slow after long time, and since the dune is increasing rapidly in volume as  $q_2$  approaches  $q_s$ , it is difficult to reliably estimate the steady-state value of  $w/W$  through numerical simulations. However, we can approximately estimate the steady-state value of  $w/W$  (which we call  $w_\infty/W$  by means of a simple calculation, as we will explain in the next paragraph.

A barchan under constant influx  $q_{in}$  is an unstable object. While the dune is gaining sand due to  $q_{in}$ , it is also losing mass through the limbs. The mass balance determines whether the dune grows or shrinks with time. As shown previously (Durán et al., 2010), there is a critical value of  $q_{in}$ , denoted by  $q_c$ , above which the dune volume increases in time and below which the dune shrinks. This critical influx is approximately equal to 18% of the saturated flux,  $q_s$  (Durán et al., 2010). The rate  $dW/dt$  at which the cross-wind width  $W$  of the barchan changes in time approximately scales with  $[q_{in} - q_c]/W$  (Durán et al., 2010). Using this relation, we can approximately estimate the growth rate of  $w$  and of  $W - w$ , which denote the fractions of the dune width under influx values  $q_2$  and  $q_1$ , respectively (cf. Fig. 6b). The growth rates  $dw/dt$  and  $d(W - w)/dt$  should be proportional to  $[q_2 - q_c]/w$  and  $[q_1 - q_c]/(W - w)$ , respectively. The steady-state value of  $w$ , i.e.  $w_\infty$  is achieved when both rates equal, which gives,

$$\frac{w_\infty}{W} = \frac{q_2 - q_c}{q_1 + q_2 - 2 \cdot q_c}, \quad (10)$$

with  $q_c \approx 0.18 q_s$  as mentioned above. Figure 7 shows how  $w_\infty/W$  depends on  $q_2/q_s$  for different values of  $q_1/q_s$ , with  $q_1, q_2 > q_c$ . For values of  $q_1$  close to  $q_c$ ,  $w_\infty/W$  approaches unity as  $q_2$  increases, which means that the dune enters al-

most entirely into the region of larger influx and is nearly symmetric again. This situation is indeed observed in the simulation (see e.g. Fig. 6a for  $q_2/q_s = 0.9$ ). However, as the influx becomes very large the barchan shape gives place to a flat dome-like dune without slip-face, which may serve as source of sand for smaller dunes (Durán et al., 2010; Luna et al., 2011, 2012). We note that an increase of  $q_1$  implies a decrease in the influx asymmetry, since  $q_2$  is within the range  $q_1 < q_2 < q_s$ . Thus, as  $q_1$  increases, the steady-state shape of the dune becomes less symmetric (though the barchan shape gives place to a dome as discussed above) and  $w_\infty/W \rightarrow 0.5$ . Evidently, for  $q_1 = q_2$  there is no asymmetry in the influx and the dune shape is thus symmetric ( $w_\infty$  is equal to  $W/2$ ).

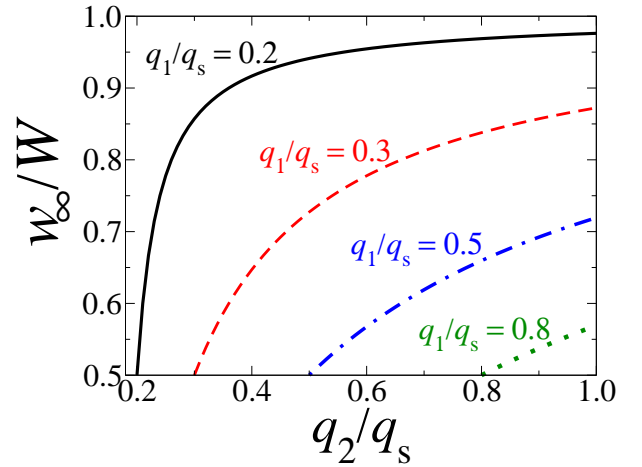


Figure 7: Steady-state value  $w_\infty/W$  of the fraction  $w/W$  of the dune cross-wind width within the region of larger influx ( $q_2$ ), as a function of  $q_2/q_s$  for different values of  $q_1/q_s$ .

## 6. Dune collisions

Dune collisions are well-known factor for the emergence of complex, asymmetric dune morphologies (Tsoar, 2001; Bourke, 2010). The dynamics of collisions between two barchans have been systematically investigated in previous studies using the present model (Schwämmle and Herrmann, 2003; Durán et al., 2005, 2009). It was shown that, if the symmetry axes of both dunes are aligned, then the collision dynamics is determined by the volume ratio of the dunes, whereas the resulting morphology is symmetric (Durán et al., 2005). However, if the collision occurs with a lateral offset (cf. Fig. 8), asymmetric dune shapes can arise (Close-Arceduc, 1969; Hersen and Douady, 2005; Durán et al., 2009).

Figure 9 shows snapshots of calculations using different values of volume ratio and lateral offset — defined as  $\Delta = |Y - y|/(W/2)$ , where  $Y$  ( $y$ ) is the crest’s position of the large (small) dune in the direction orthogonal to the wind, and  $W$  is the width of the large dune (Fig. 8).

The asymmetric dune shapes produced due to collisions are different from the ones in Section 5, since the collision not only implies an asymmetric influx but also leads to a (dynamic) modification in the shear stress field during the interaction between the dunes (Durán et al., 2005). The hybrid, asymmetric dunes depicted in Fig. 9 are transient shapes. A sufficiently long time after the collision, dunes are well separated and adapt to constant influx and wind direction again.

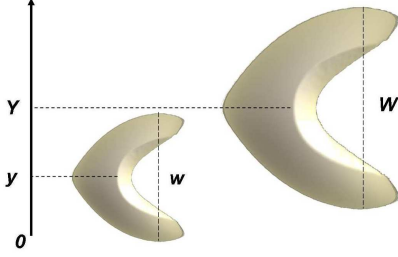


Figure 8: Binary collision between barchans of different sizes. A small barchan (width  $w$ ) approaches a larger one (width  $W$ ) from behind with lateral offset. The small and the large barchans are centered at  $y$  and  $Y$ , respectively.



Figure 9: Snapshots of simulations of binary collisions for different values of  $\Delta$  and volume ratio  $r \propto (w/W)^3$ . Calculations with  $r = 0.06$  are shown for (a)  $\Delta = 0.2$ , (c)  $\Delta = 0.6$  and (e)  $\Delta = 0.9$ ; calculations with  $r = 0.3$  are shown for (b)  $\Delta = 0.2$ , (d)  $\Delta = 0.6$  and (f)  $\Delta = 0.9$ .

The simulations corroborate previous observations that dune asymmetry could result from limb merging as two barchans link laterally, thereby causing downwind extension of the coalesced limbs (Bourke, 2010). Such a situation is found for sufficiently large offset ( $\Delta > 0.9$ ), as can be seen in Figs. 9e and 9f. It is interesting to notice that the result of the lateral coalescence is the release of a

small dune from the merged limbs, whereas the colliding barchans merge then into a single asymmetric dune. For other values of  $\Delta$ , asymmetric barchan shapes can form during the separation of the barchans resulting from the collisional interaction. However, no limb extension occurs as the faster barchan upwind is approaching the larger one downwind.

Asymmetric dune patterns very different from the ones in Fig. 9 can result from collisions between multiple dunes. Figure 10a shows one snapshot of the simulation of a barchan dune field emerging from a flat sand surface subjected to a saturated influx. The simulations of the genesis of barchan fields were discussed in detail in previous works (Durán et al., 2010; Luna et al., 2011, 2012). As shown in these works, the small transverse bedforms emerging from the instabilities which develop on the flat hill upwind give place to small barchans after reaching the bedrock — due to the cross-wind instability inherent to transverse dunes (Reffet et al., 2010; Parteli et al., 2011; Melo et al., 2012; Niiya et al., 2012). The barchan dunes, which are subjected to a strong influx, grow in size during their migration, thereby experiencing multiple collisions with their counterparts and producing complex, asymmetric dune shapes. Different patterns produced in the simulation include limb extension of the upwind barchan, as we can see in Fig. 10a. While the simulation of Fig. 10a denotes a model for an immature dune field (which is at the early stages of its development), we have also performed simulations using periodic boundary conditions in the wind direction such as to model the steady-state dynamics of a dune corridor (Durán et al., 2010). Such simulations also lead to asymmetric barchan shapes which cannot be obtained with binary collisions (cf. Fig. 10b).

The complex asymmetric shapes shown in Figs. 10a and 10b result from collisions between multiple barchans which have different sizes and offset values, and are further subjected to an asymmetric influx depending on the spatial distribution of dunes upwind. The systematic study of collisions between multiple dunes in a field is out of the scope of the present study. However, on the basis of our calculations, we can conclude that binary collisions can produce a rather limited range of asymmetric dune patterns. The only previously reported asymmetric pattern produced by a binary collision is the limb elongation due to dunes merging laterally (Fig. 9e,f). Other asymmetric patterns induced by collisions can result if the collisions involve multiple dunes during the evolution of a barchan dune field. As can be seen in Figs. 10a and 10b, collisions between dunes lead to the formation of groups of barchans, in which upwind barchans releasing sand through their extended limbs act as source of sediment to the dunes in the front, as previously noted by Tsoar (2001). Indeed, the complex patterns emerging from collisions between barchans are transient dune shapes, as shown in Fig. 9 and in previous works (Schwämmle and Herrmann, 2003; Durán et al., 2005, 2010). Further modeling work is required in order to deepen our understanding of the colli-

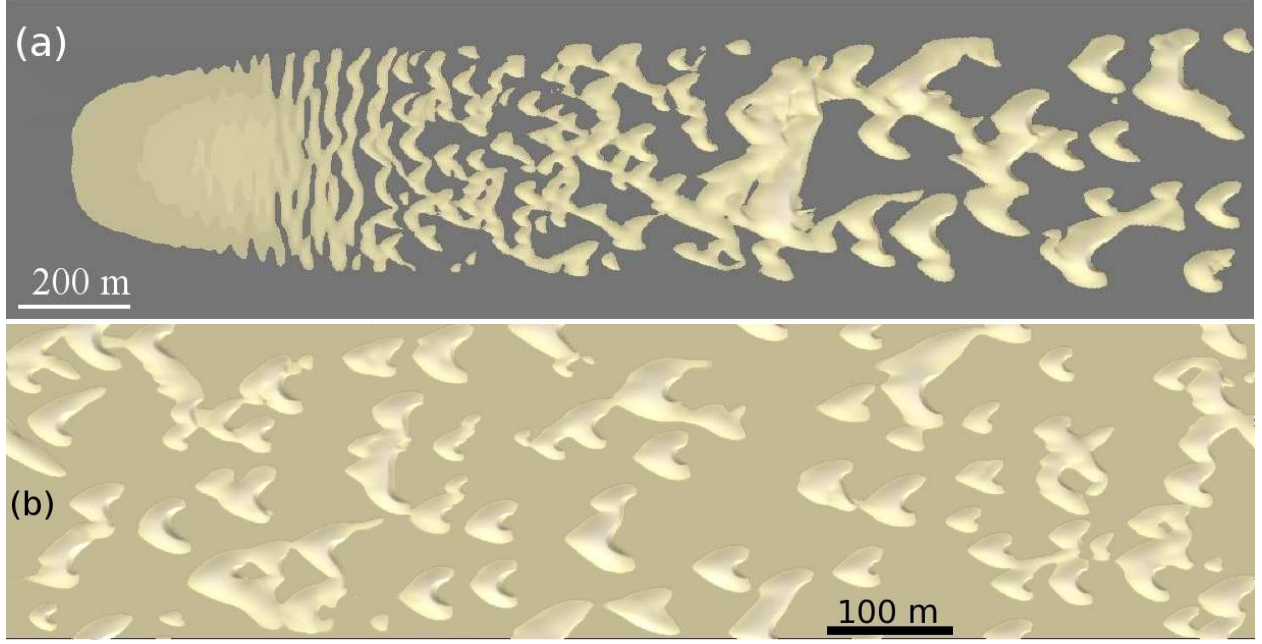


Figure 10: Asymmetric barchans emerge during the evolution of a barchan dune field. (a) Simulation of the genesis of a dune field. A small, flat sand hill subjected to saturated flux becomes a source of sand for a barchan dune field (Durán et al., 2010; Luna et al., 2012). Collision between multiple dunes lead to complex asymmetric dune morphologies which are not obtained in binary collisions (cf. Fig. 9). (b) Complex asymmetric barchan shapes also occur in the simulation of a barchan corridor using periodic boundary conditions both in the direction perpendicular and parallel to the wind. Wind blows from left to right in both (a) and (b). Simulations were performed with  $\tau/\tau_t \approx 3.9$ .

sion dynamics of multiple dunes and of the resulting dune patterns.

## 7. Conclusions

In conclusion, we have investigated, by means of morphodynamic modeling of aeolian dunes, the respective roles of bimodal wind regimes, topography, influx asymmetry and dune collisions on the formation and evolution of asymmetric barchan dune shapes. The conclusions of our numerical simulations can be summarized as follows:

- *Bimodal wind regimes* — the limb opposite to the secondary wind elongates into the resultant transport direction if the divergence angle of the bimodal wind is obtuse and the ratio  $[Q_2 T_{w2}]/[Q_1 T_{w1}]$  — where  $Q_1$  ( $Q_2$ ) and  $T_{w1}$  ( $T_{w2}$ ) stand for the bulk sand flux and the duration of the primary (secondary) wind, respectively — exceeds 25%. These conditions are the same as the ones for oblique alignment of bedforms in dense sand beds (Rubin and Hunter, 1987), the asymmetric barchan being the corresponding morphology under low amount of available sand.
- *Topography* — a barchan crossing a topographic rise can become asymmetric; the limb closest to the topographic rise elongates downwind. The migration velocity of a barchan that is on a tilted surface has a

downhill component proportional to the tilting slope; the preferential limb extension is downhill rather than downwind.

- *Influx asymmetry* — the side of the barchan subjected to the larger influx increases in volume, whereas the opposite limb elongates downwind. The typical asymmetric morphology is a barchan with an elongated arm (the one subjected to lower influx). The asymmetry is of transient nature, since the dune migrates laterally towards the region of higher influx.
- *Dune collisions* — asymmetry can be triggered due to barchan collisions with lateral offset. Binary collisions with large offset can lead to extension of the limb resulting from the merging of the two limbs participating at the collision. Collisions between multiple barchans in a field can trigger more complex asymmetric patterns. Some patterns produced in these simulations involve the elongation of one limb of the upwind dune, as reported from previous observations (Bourke, 2010).

In order to improve the quantitative assessment of asymmetric barchans, the model should be extended in order to account for secondary flow effects at the dune lee (Tsoar, 2001), which may be relevant for the dynamics of limb elongation due to bimodal wind regimes or due to topo-

graphic ridges with sharp slopes (Bourke, 2010). Furthermore, realistic simulations of bimodal wind regimes should account for multiple secondary wind trends in consistence with the complex sand roses of real dune fields (Fryberger and Dean, 1979). The results of our calculations are potentially useful for inferring local wind regimes or spatial variations either in topography or in availability of mobile sediments in planetary dune fields where asymmetric barchans occur.

## Acknowledgments

This work was supported in part by NASA MDAP Grant NNX10AQ35G, by FUNCAP, CAPES and CNPq (Brazilian agencies), by Swiss National Foundation Grant NF 20021-116050/1 and ETH Grant ETH-10 09-2. EJP thanks the German Research Foundation (DFG) for funding through the Cluster of Excellence “Engineering of Advanced Materials” and FUNCAP Grant 0011-00204.01.00/09 for partial support during execution of this work in Fortaleza.

## References

- Allen, J.R.L., 1974. Reaction, relaxation and lag in natural sedimentary systems: General principles, examples and lessons. *Earth Sci. Rev.* 10, 263-342.
- Almeida, M.P., Parteli, E.J.R., Andrade Jr., J.S., Herrmann, H.J., 2008. Giant saltation on Mars. *Proc. Natl. Acad. Sci.* 105, 6222-6226.
- Andreotti, B., 2004. A two-species model of aeolian sand transport. *Journal of Fluid Mechanics* 510, 47-70.
- Bagnold, R.A., 1941. *Physics of blown sand and desert dunes*. Methuen, London, 289 pp.
- Bourke, M.C., Balme, M., Zimbelman, J.R., 2004. A comparative analysis of barchan dunes in the intra-crater dune fields and the North Polar Sand Sea, LPSC XXXV abstr. #1453.
- Bourke, M.C., 2010. Barchan dune asymmetry: Observations from Mars and Earth. *Icarus* 205, 183-197.
- Bourke, M.C., Goudie, A.S., 2009. Varieties of barchan dunes in the Namib Desert and on Mars. *Aeolian Research* 1, 45-54.
- Bourke, M.C., Lancaster, N., Fenton, L.K., Parteli, E.J.R., Zimbelman, J.R., Radebaugh, J., 2010. Extraterrestrial dunes: An introduction to the special issue on planetary dune systems. *Geomorphology* 121, 1-14.
- Bristow, C.S., Bailey, S.D., Lancaster, N., 2000. The sedimentary structure of linear sand dunes. *Nature* 406, 56-59.
- Close-Arceud, A. *Essai d'explication des formes dunaires sahariennes. Etudes de Photo-Interpretation*. Institut Geographique National, 1969.
- De Hon RA, 2006. Transitional Dune Forms on Mars. *Proc. Lunar Planet. Sci. Conf.* 37, #1361.
- Dong, Z., Wei, Z., Qian, G., Zhang, Z., Luo, W., Hu, G., 2010. “Raked” linear dunes in the Kumtagh Desert, China. *Geomorphology* 123, 122-128.
- Durán, O., Schwämmle, V. and Herrmann, H.J., 2005. Breeding and solitary wave behavior of dunes. *Physical Review E* 72, 021308.
- Durán, O., Herrmann, H.J., 2006a. Modelling of saturated sand flux. *Journal of Statistical Mechanics: Theory and Experiment*, P07011.
- Durán, O., Herrmann, H.J., 2006b. Vegetation against dune mobility. *Physical Review Letters* 97, 188001.
- Durán, O., Schwämmle, V., Lind, P.G., Herrmann, H.J., 2009. The dune size distribution and scaling relations of barchan dune fields. *Granular Matter* 11, 7-11.
- Durán, O., Parteli, E.J.R., Herrmann, H.J., 2010. A continuous model for sand dunes: Review, new developments and application to barchan dunes and barchan dune fields. *Earth Surface Process and Landforms* 35, 1591-1600 (2010). doi:10.1002/esp.2070.
- Durán, O., Claudin, P., Andreotti, B., 2011. On aeolian transport: Grain-scale interactions, dynamical mechanisms and scaling laws. *Aeolian Research* 3, 243-270.
- Elbelrhiti, H., Claudin, P., Andreotti, B., 2005. Field evidence for surface-wave-induced instability of sand dunes. *Nature*, 437, 720-723.
- Finkel, H.J., 1959. The barchans of southern Peru. *J. Geol.* 67, 614-647.
- Fryberger, S.G., Dean, G., 1979. A Study of Global Sand Seas.. In: McKee, E.D. (Ed.), *U.S. Geol. Surv. Prof. Pap.*, 1052. U.S. Geological Survey, Reston, VA, pp. 137-169.
- Fryberger, S.G., Al-Sari, A.M., Clisham, T.J., Rizvi, S.A.R., Al-Hinai, K.G., 1984. Wind sedimentation in the Jafurah sand sea, Saudi Arabia. *Sedimentology* 31, 413-431.
- Gay, S.P., 1999. Observations regarding the movement of barchan sand dunes in the Nazca to Tanaca area of southern Peru. *Geomorphology* 27, 279-293.
- Goudie, A., Wilkinson, J., 1977. *The warm desert environment*. Cambridge Univ. Press, Cambridge, 88 pp.
- Herrmann, H.J., Andrade Jr., J.S., Schatz, V., Sauermann, G., Parteli, E.J.R., 2005. Calculation of the separation streamlines of barchans and transverse dunes. *Physica A* 357, 44-49.
- Hersen, P., Andersen, K.H., Elbelrhiti, H., Andreotti, B., Claudin, P., Douady, S., 2004. Corridors of barchan dunes: Stability and size selection. *Physical Review E* 69, 011304.
- Hersen, P., Douady, S., 2005. Collision of barchan dunes as a mechanism of size regulation. *Geophys. Res. Lett.* 32, 1-5.
- Kok, J.F., Parteli, E.J.R., Michaels, T.I., Bou Karam, D., 2012. The physics of wind-blown sand and dust. *Reports on Progress in Physics* 75, 106901.
- Kroy, K., Sauermann, G., Herrmann, H.J., 2002. Minimal model for aeolian sand dunes. *Physical Review E* 66, 031302.
- Lancaster, N., 1980. The formation of seif dunes from barchans — supporting evidence for Bagnold’s model from the Namib Desert. *Zeitschrift für Geomorphologie N.F.* 24, 160-167.
- Lancaster, N., 1982. Dunes on the Skeleton Coast, Namibia (south west Africa): Geomorphology and grain size relationships. *Earth Surf. Proc. Land.* 7, 575-587.
- Lancaster, N., 1988. The development of large aeolian bedforms. *Sediment Geology* 55, 69-89.
- Long, J.T., Sharp, R.P., 1964. Barchan-dune movement in Imperial Valley, California. *Geol. Soc. Am. Bull.* 75, 149-156.
- Luna, M.C.M.M., Parteli, E.J.R., Durán, O., Herrmann, H.J., 2011. Model for the genesis of coastal dune fields with vegetation. *Geomorphology* 129, 215-224.
- Luna, M.C.M.M., Parteli, E.J.R., Herrmann, H.J., 2012. Model for a dune field with an exposed water table. *Geomorphology* 159-160, 169-177.
- Mabbutt, J.A., 1977. *Desert Landforms* (MIT Press, Cambridge), 340 pp.
- McKee, E., Tibbitts, G.C., Jr., 1964. Primary structures of a seif dune and associated deposits in Libya. *Journal of Sedimentary Petrology* 34, 5-17.
- Melo, H.P.M., Parteli, E.J.R., Andrade Jr., J.S., Herrmann H.J., 2012. Linear stability analysis of transverse dunes. *Physica A* 391, 4606-4614.
- Niiya, H., Awazu, A., Nishimori, H., 2012. Bifurcation analysis of the transition of dune shapes under a unidirectional wind. *Physical Review Letters* 108, 158001.
- Owen, P.R., 1964. Saltation of uniform grains in air. *Journal of Fluid Mechanics* 20, 225-242.
- Parteli, E.J.R., Schwämmle, V., Herrmann, H.J., Monteiro, L.H.U., Maia, L.P., 2006. Profile measurement and simulation of a transverse dune field in the Lencois Maranhenses. *Geomorphology* 81, 29-42.
- Parteli, E.J.R., Durán, O., Herrmann, H.J., 2007. Minimal size of a barchan dune. *Physical Review E* 75, 011301.

- Parteli, E.J.R., Herrmann, H.J., 2007. Saltation transport on Mars. *Physical Review Letters* 98, 198001.
- Parteli, E.J.R., Durán, P., Tsoar, H., Schwämmle, V., Herrmann, H.J., 2009. Dune formation under bimodal winds. *Proc. Nat. Acad. Sci.* 106, 22085-22089.
- Parteli, E.J.R., Andrade Jr., J. S., Herrmann, H.J., 2011. Transverse instability of dunes. *Physical Review Letters* 107, 188001.
- Pähtz, T., Kok, J.F., Herrmann, H.J., 2012. The apparent roughness of a sand surface blown by wind from an analytical model of saltation. *New Journal of Physics* 14, A262.
- Reffet, E., Courrech du Pont, S., Hersen, P., Douady, S., 2010. Formation and stability of transverse and longitudinal sand dunes. *Geology* 38, 491-494.
- Rim, S.C.R., 1958. Simulations by dynamical model, of sand tract morphology occurring in Israel. *Bull. Res. Counc. Israel* 7-G, 123-137.
- Rubin D.M., Hunter R.E., 1987. Bedform alignment in directionally varying flows. *Science* 237, 276-278.
- Rubin D.M., Ikeda, H., 1990. Flume experiments on the alignment of transverse, oblique, and longitudinal dunes in directionally varying flows. *Sedimentology* 37, 673-684.
- Rubin, D.M., Tsoar, H., Blumberg, D.G., 2008. A second look at western Sinai seif dunes and their lateral migration. *Geomorphology* 93, 335-342.
- Ruhe, R.V., 1975. *Geomorphology*. Houghton Mifflin, Boston, 246 pp.
- Sauermann, G., Kroy, K., Herrmann, H.J., 2001. A continuum saltation model for sand dunes. *Physical Review E* 64, 31305.
- Sauermann, G., Andrade Jr., J.S., Maia, L.P., Costa, U.M.S., Araújo, A.D., Herrmann, H.J., 2003. Wind velocity and sand transport on a barchan dune. *Geomorphology* 54, 245-255.
- Schwämmle, V., Herrmann, H.J., 2003. *Nature* 426, 619-620 (2003).
- Tokano, T., 2010. Relevance of fast westerlies at equinox for the eastward elongation of Titan's dunes. *Aeolian Research* 2, 113-127.
- Tsoar, H., 1982. Internal structure and surface geometry of longitudinal (seif) dunes. *J. Sediment. Petrol.* 52, 823-831.
- Tsoar, H., 1983. Dynamic processes acting on a longitudinal (seif) sand dune. *Sedimentology* 30, 567-578.
- Tsoar, H., 1984. The formation of seif dunes from barchans — a discussion. *Zeitschrift für Geomorphologie* 28, 99-103.
- Tsoar, H., 2001. Types of Aeolian Sand Dunes and Their Formation. *Geomorphological Fluid Mechanics* 582, 403-429.
- Verstappen, H.Th., 1968. On the origin of longitudinal (seif) dunes. *Zeitschrift für Geomorphologie N.F.* 12, 200-220.
- Walker, I.J., Nickling, W.G., 2002. Dynamics of secondary airflow and sediment transport over and in the lee of transverse dunes. *Progress in Physical Geography* 26, 47-75.
- Weng, W.S., Hunt, J.C.R., Carruthers, D.J., Warren, A., Wiggs, G.F.S., Livingstone, I., Castro, I., 1991. Air flow and sand transport over sanddunes. *Acta Mechanica, Suppl.* 2, 1-22.